OPEN ACCESS
IOP Publishing
Journal of Physics D: Applied Physics
J. Phys. D: Appl. Phys. **54** (2021) 025107 (7pp)
https://doi.org/10.1088/1361-6463/abbc37

Influence of micro-patterning of the growth template on defect reduction and optical properties of non-polar $(11\bar{2}0)$ GaN

Jochen Bruckbauer[1], Yipin Gong[2], Ling Jiu[2], Michael J Wallace[1], Anja Ipsen[3], Sebastian Bauer[3], Raphael Müller[3], Jie Bai[2], Klaus Thonke[3], Tao Wang[2], Carol Trager-Cowan[1] and Robert W Martin[1]

[1] Department of Physics, SUPA, University of Strathclyde, Glasgow G4 0NG, Scotland, United Kingdom
[2] Department of Electronic and Electrical Engineering, University of Sheffield, Sheffield S1 3JD, United Kingdom
[3] Semiconductor Physics Group, Institute of Quantum Matter, Ulm University, D-89081 Ulm, Germany

E-mail: jochen.bruckbauer@strath.ac.uk

Received 8 July 2020, revised 14 September 2020
Accepted for publication 28 September 2020
Published 20 October 2020

Abstract

We investigate the influence of different types of template micro-patterning on defect reduction and optical properties of non-polar GaN using detailed luminescence studies. Non-polar $(11\bar{2}0)$ (or *a*-plane) GaN exhibits a range of different extended defects compared with its more commonly used *c*-plane counterpart. In order to reduce the number of defects and investigate their impact on luminescence uniformity, non-polar GaN was overgrown on four different GaN microstructures. The micro-patterned structures consist of a regular microrod array; a microrod array where the $-c$-side of the microrods has been etched to suppress defect generation; etched periodic stripes and finally a subsequent combination of etched stripes and etched microrods (double overgrowth). Overall the presence of extended defects, namely threading dislocations and stacking faults (SFs) is greatly reduced for the two samples containing stripes compared with the two microrod samples. This is evidenced by more uniform emission and reduction in dark regions of non-radiative recombination in room temperature cathodoluminescence imaging as well as a reduction of the SF emission line in low temperature photoluminescence. The observed energy shifts of the GaN near band edge emission are related to anisotropic strain relaxation occurring during the overgrowth on these microstructures. A combination of stripes and microrods is a promising approach for defect reduction and emission uniformity in non-polar GaN for applications in light-emitting devices as well as power electronics.

Keywords: cathodoluminescence, non-polar GaN, nitride semiconductors, scanning electron microscopy

(Some figures may appear in colour only in the online journal)

1. Introduction

Since the scientific breakthroughs in the late 1980s and early 1990s, III-nitride-based (opto)electronic devices have revolutionised the electronics industry, in particular, the field of solid-state lighting [1]. However, most commercially

available nitride-based devices are grown along the polar *c*- or [0001] direction, which ultimately limits their performance due to large internal electric fields induced by spontaneous and piezoelectric polarisation [2].

For light-emitting diodes and laser diodes, which contain a (multiple) quantum well structure, the polarisation-induced internal electric field leads to the quantum-confined Stark effect, which can have a detrimental effect on device efficiency [3]. In AlGaN/GaN heterojunction field-effect transistors, the polarisation fields lead to the formation of a two-dimensional electron gas at the heterointerface, which is utilised for on state (or depletion mode) devices for power switching applications. For safe operation, however, normally off state (or enhancement mode) devices would be favourable [4].

There are several alternative routes to address the above issues, which include the use of nano- and microstructures, zinc-blende GaN or growth along a different crystal direction, such as semi- and non-polar orientations, the latter being the topic of this letter.

Growing III-nitrides in a non-polar orientation, however, comes with its own challenges. Compared with their polar counterparts, moving to non-polar orientations introduces additional extended defects such as basal-plane and prismatic stacking faults (SFs) and misfit dislocations in addition to the commonly observed threading dislocations (TDs). Homoepitaxy on native substrates allows high quality GaN epilayers, however, these substrates are generally very small and expensive, which makes this an unsuitable approach for cost-effective industrial mass production. An alternative, more economical approach is to use foreign substrates, such as sapphire or silicon, which unfortunately leads to high densities of these extended defects.

In order to reduce the density of defects and hence to improve crystal quality, epitaxial lateral overgrowth can be used, which has been successfully employed for *c*-oriented GaN, generally using a *stripe* pattern [5–8]. However, for non-polar orientations the growth dynamics need to be carefully considered due to the different crystal orientations and associated growth rates in order to achieve smooth and coalesced surfaces. In order to address the different growth rates and defect formation in non-/semi-polar materials, overgrowth is performed on micro-patterned GaN templates. The geometry of the patterning has a major impact. This approach has been successfully demonstrated to achieve high quality semi-polar $(11\bar{2}2)$ GaN on *m*-plane sapphire, where an initial GaN layer was patterned into a regular array of *microrods* for subsequent overgrowth [9, 10]. Alternatively, overgrowth using an array of nanocolumns produced by selective area growth is a promising route to fabricate high quality semi- and non-polar films, also referred to as pseudo-substrates [11, 12].

Carrier recombination at extended defects (such as TDs, SFs or misfit dislocations) at room temperature (RT) generally occurs through non-radiative recombination processes leading to suppressed light emission [13–15]. For example, dislocations can act as charged line defects attracting minority carriers, which then recombine non-radiatively at the defect [16]. To visualise and investigate the lateral distribution of these extended defects highly spatially-resolved imaging techniques, such as cathodoluminescence (CL), can be employed, where the defects appear as dark features [17]. CL imaging is a powerful and established tool to rapidly and non-destructively investigate the luminescence properties of light-emitting materials providing information on defects, composition, doping and strain [18].

In this letter, we probe the luminescence properties of non-polar $(11\bar{2}0)$ (or *a*-plane) GaN overgrown on different GaN microstructures using CL imaging and photoluminescence (PL) spectroscopy in order to investigate the influence of micro-patterning on the presence of defects and spatial uniformity in emission intensity. A series of four different types of micro-pattern are considered: a regular microrod array, etched microrods ('mushroom configuration'), periodic stripes and a combination of stripes and microrods ('double overgrowth').

2. Experimental section

The growth and fabrication of the non-polar GaN samples consists of three steps. First, initial growth of a continuous non-polar GaN layer on *r*-plane sapphire. Second, fabrication of the different microstructures through various etching processes. Third, overgrowth of these microstructures until the GaN layer coalesces.

In the first step, non-polar $(11\bar{2}0)$ GaN is grown by metalorganic chemical vapour deposition (MOCVD) on *r*-plane sapphire substrates using a high temperature AlN buffer [19]. The approximate thickness of this epilayer is 1–1.3 μm depending on the sample.

Subsequently, these epilayers serve as templates for the fabrication of the different microstructures. A SiO_2 layer is patterned into microrods or stripes using a standard photolithography technique and dry-etching processes employing reactive ion etching. The patterned SiO_2 layer then serves as a mask to etch the GaN down to the sapphire substrate using a standard inductively coupled etching process. The first sample for the later overgrowth is simply a regular, square microrod array in a chess-board pattern with microrod diameters and pitch both of 4 μm. The diagonal directions in the square chess-board arrangement align to the [0001] and $[1\bar{1}00]$ direction, respectively, as shown in the secondary electron (SE) micrograph in figure 1(a). The other microstructures undergo an additional etching step in order to reduce defect generation. Overgrowth of semi-polar and non-polar GaN in general leads to defect-free material in the [0001] or *c*-direction, whereas the $[000\bar{1}]$ or $-c$-direction allows defects to penetrate to the surface [20, 21]. For this reason the $-c$-side of the microstructures is etched in order to suppress growth along this $-c$-direction. This is achieved by photo-enhanced chemical etching using a 10% KOH solution, which only effectively etches the N-face on the $-c$-side of the microstructure, but leaves the Ga-face of the *c*-side unaffected. The second microstructure is a microrod array (microrod diameter and pitch both of 2.5 μm) which has undergone this etching process resulting in a regular, etched microrod array in the so-called 'mushroom configuration' as seen in the cross-section SE image in figure 1(b). The third microstructure consists of periodic stripes of 1.5 μm width and

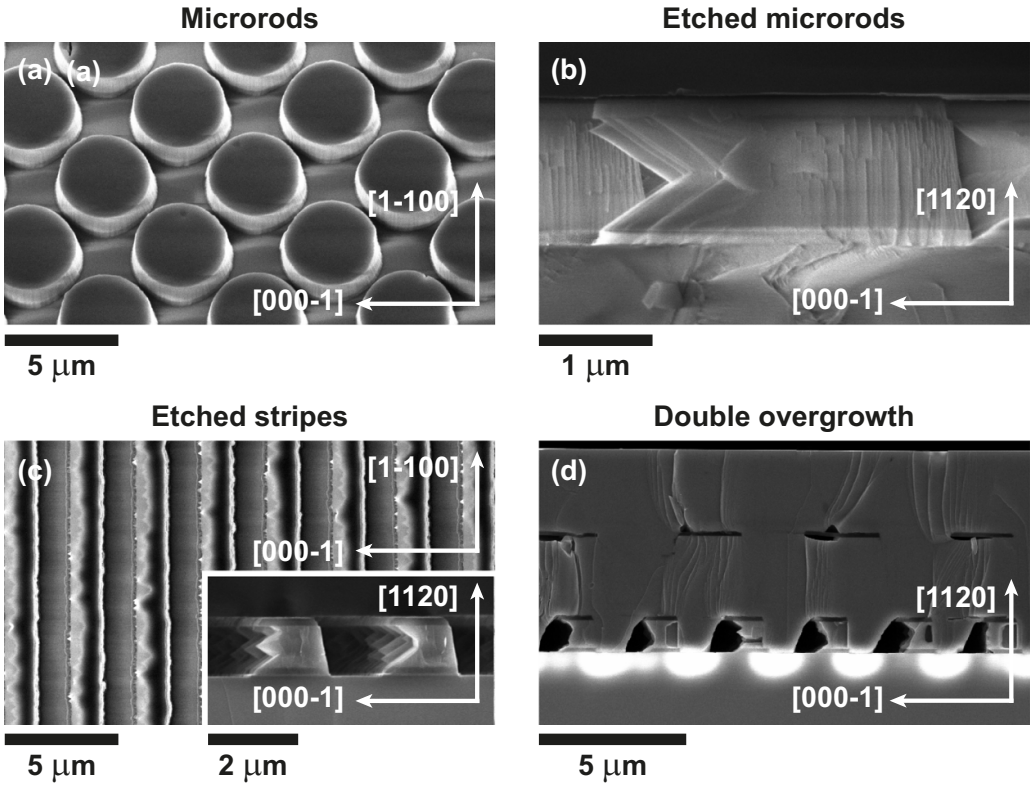

Figure 1. SE images of the four different GaN microstructures before overgrowth (except (d)): (a) top-view of regular microrod array (4 μm diameter and pitch), (b) cross-section of etched microrod array in mushroom configuration (2.5 μm diameter and pitch), (c) top-view and cross-section (inset) of etched stripes (1.5 μm strip and gap width) and (d) cross-section of the double overgrowth sample after the entire growth using etched stripes (2.5 μm diameter and pitch) followed by etched microrods (1.5 μm stripe and gap width). The darker layers in the cross-section images are parts of the SiO_2 mask.

gap with the stripes aligned along the $[1\bar{1}00]$ direction, which have also been partially etched on the $-c$-side as displayed in figure 1(c). The fourth type of samples uses a combination of the previous two microstructures, where a first overgrowth uses etched stripes (1.5 μm width and gap) and is followed by a second overgrowth on etched microrods (microrod diameter and pitch of 2.5 μm). A cross-section SE image of the double overgrowth structure is shown in figure 1(d). In all cases, the SiO_2 mask has been left on top of the etched microstructure.

Finally, the third step consists of further MOCVD overgrowth until a coalesced layer has formed. The total sample thickness is several microns depending on the microstructure. Different sets of samples were produced to optimise growth and fabrication parameters for each micro-pattern and each sample is one of the best from the relevant set. The growth and fabrication of the etched microrod arrays (mushroom configuration), stripes and double overgrowth samples are further described in [22, 23].

Non-polar GaN grown on *r*-plane sapphire substrates has the inherent issue of anisotropic strain within the growth plane due to the lack of six-fold symmetry for the $(11\bar{2}0)$ orientation [24]. This is caused by the different lattice mismatches between *r*-plane sapphire and $(11\bar{2}0)$ GaN along the [0001] and $[1\bar{1}00]$ directions (*c*- and *m*-directions, respectively), which are the two in-plane directions. It has been shown previously by high resolution x-ray diffraction (HRXRD) that strain in $(11\bar{2}0)$ GaN can be influenced by the overgrowth of GaN microstructures, such as regular microrods or periodic stripes [22, 23]. This is due to the formation of voids leading to strain relaxation [22]. The samples overgrown on microrods exhibit anisotropic strain due to these voids forming along all in-plane directions. The samples overgrown on the stripes only show anisotropic strain in the direction perpendicular to the stripes as voids can only form between the stripes.

RT CL hyperspectral imaging was performed in a variable pressure field emission scanning electron microscope (FEI Quanta 250) [25]. For every pixel in the image, a spectrally-resolved luminescence spectrum is collected with a spatial resolution approaching 10 nm [14]. The emitted light from the sample, which is tilted by 45°, is collected by a Schwarzschild reflecting objective with its optical axis perpendicular to the direction of the electron beam, dispersed with a 1/8 m focal length spectrometer (Oriel MS125) and collected using a 1600-channel electron multiplying charge-coupled device (CCD, Andor Newton). The CL data presented here were acquired with an electron beam energy of 5 keV giving an excitation volume with approximate radius of order of 100 nm. For the variable temperature PL measurements the samples were placed inside a liquid helium flow cryostat. A monochromator (SPEX1704) with a 1 m focal length and liquid nitrogen-cooled CCD were used for the detection of the emitted luminescence, which was excited by the 325 nm

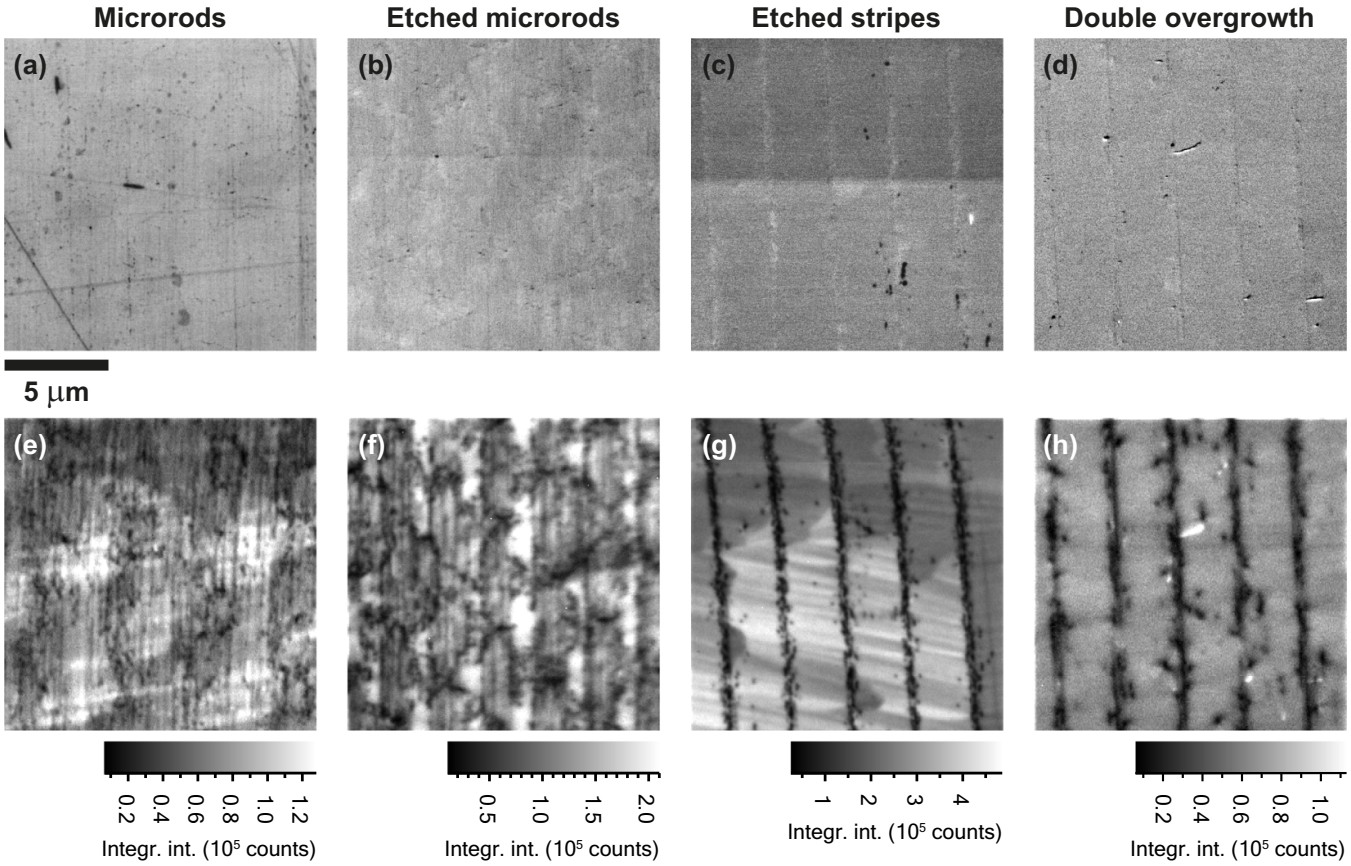

Figure 2. SE images and integrated CL intensity images of the GaN NBE emission of GaN overgrown on (a), (e) a microrod array, (b), (f) etched microrod array, (c), (g) a stripe pattern and (d), (h) combination of stripes and microrods, respectively. The intensities between the samples are not comparable due to slight differences in the measurement set-up. The intensity scales are adjusted to ±90% of the mean intensity value. The scale bar in (a) applies to all SE and CL images.

line of a He-Cd laser. The spectra were not corrected for the wavelength response of the detection system, which exhibits a negligible change over this short wavelength range below 400 nm.

3. Results and discussion

The spatial uniformity over relatively large areas (15×15 μm^2) was investigated using RT CL imaging of GaN epilayers grown using the four different microstructures for overgrowth. The CL images of the integrated intensity of the GaN near band edge (NBE) emission together with the SE image of the area imaged by CL are shown in figure 2. The intensity scale for each of the CL images was chosen to be ±90% of the mean intensity value for relative comparison.

The surfaces for both microrod samples appear smooth, except for a few scratches, as seen in the SE images in figure 2(a) and (b). On the other hand, the SE images for the etched stripe and double overgrowth samples, figures 2(c) and (d), exhibit periodic faint lines with a separation of about 3 μm. The separation corresponds well with the pitch of the etched stripes (1.5 μm stripe and gap width). Additionally, small pits and trenches are observed for the double overgrowth epilayer.

The integrated intensity images of the GaN NBE emission in figures 2(e)–(h) demonstrate very clearly the impact of the different types of micro-pattern on the spatial dependence of emission from the overgrown GaN. The most non-uniform emission is shown by the epilayers overgrown on the two different microrod structures. However, several periodic patterns can be discerned in the CL intensity images in figures 2(e) and (f). The regular microrod sample (figure 2(e)) exhibits parallel black lines (vertical), circles of black dots and circular regions of brighter intensity. The black dots and lines are associated with non-radiative recombination at TDs and basal-plane stacking faults at RT [7, 15, 26]. The etched microrod sample (figure 2(f)) also shows parallel black lines, black dots and brighter areas. It it noticeable that the black dots in the regular microrod sample mostly appear as circles of black dots. The periodicity of these circles match the dimensions and pitch of the microrods (4 μm). Whereas for the etched microrod sample, the arrangement of black dots appears less circular. These features also approximately match the dimensions and pitch of the etched microrods (2.5 μm).

The GaN CL intensity images for the two samples employing stripes for the overgrowth are very different compared to the microrod approach. The etched stripe sample (figure 2(g)) exhibits dark bands of closely spaced black dots, separated by regions of mostly uniform intensity. Some dark spots also appear in these brighter, uniform bands. The separation between the dark bands corresponds to the pitch of the etched

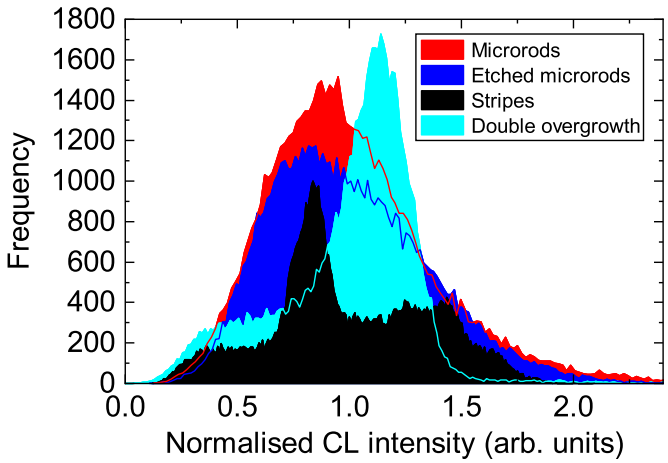

Figure 3. Histogram of the intensities from the CL intensity images of the GaN NBE emission in figures 2(e)–(h). The intensities are normalised using their respective mean intensity for comparison.

stripes and also to the vertical lines visible in the SE image of the same area in figure 2(c). The uniform regions can be divided into two regions, one slightly brighter than the other and both extending over several dark bands. A single faint dark line, parallel to the dark bands is visible on the right hand side of figure 2(g). The double overgrowth sample (figure 2(h)) is very similar to the stripe-only overgrowth sample. However, the bands of dark spots appear denser and the black dots are less distinguishable. Similarly, the individual black spots in the brighter and mostly uniform bands appear larger. Again, the stripe separation corresponds to the 3 μm pitch of the overgrown stripes and coincides with the vertical lines in the SE image of the same area in figure 2(d). Although, the double overgrowth sample employs etched microrods in a second overgrowth step, the overall luminescence is mostly influenced by the overgrowth of the stripes below the microrods. This indicates that the stripe overgrowth is much more effective in reducing the defect density compared with the microrod approach.

The intensity histograms of the CL intensity images in figures 2(e)–(h) are shown in figure 3, where the CL intensities have been normalised using their respective mean intensity in order to make a meaningful comparison of the intensity distributions. The lateral intensity distributions observed in the CL intensity images are very well reflected in the histograms. The regular and etched microrods samples have a fairly broad bell-shaped curve with a longer tail on the higher intensity side reflecting the larger range of intensities present in those two samples.

The distribution for the stripe sample consists of three contributions, which can be associated with two distinct areas in the sample. The two highest intensities are associated with the wide bright stripe in the CL image in figure 2(g). However, this bright stripe can be subdivided into two intensity regions, the slightly less bright one showing the highest occurrence of intensities is close to the mean intensity and a brighter region with a wider range of intensities. The third contribution is associated with the narrower dark lines of closely spaced dark spots. The histogram for the double overgrowth sample is more similar to that from the stripe sample than to the bell-shaped curves for the microrod samples. The main contribution is from the bright stripe, which in this case only consists of intensity near the mean intensity for that sample. The second lower intensity peak is from the narrow lines of dark spots.

Overall, the benefit of the double overgrowth on emission uniformity can be clearly seen in the CL intensity image (figure 2(f)) and corresponding histogram (figure 3). Although the double overgrowth still employs etched microrods for the overgrowth, the luminescence is much more uniform. The overgrowth on the etched microrods happens after the overgrowth on the stripes. This means that the stripes are very efficient in reducing the density of extended defects. Subsequent overgrowth in the etched microrods further improves the uniformity.

So far only the spatial luminescence properties of these overgrowth GaN samples have been considered. To further investigate the optical properties, the spectrally-resolved emission from large areas is recorded. Figure 4(a) shows the RT mean CL spectra calculated from the hyperspectral CL data used to generate the CL intensity images in figures 2(e)–(h). The spectra have been normalised to the GaN NBE emission peak in order to compare their spectral emission profiles. Two effects of the different micro-patterning can be seen in the CL emission spectra. First, the GaN NBE emission is shifted and second, the lower energy shoulders exhibit different intensities for the four different samples.

The shift in GaN NBE peak position can be associated with a different overall strain in the epilayers. It is generally known that strain shifts the band gap of the material. In this case, the sample overgrown on the stripes has the lowest NBE emission energy followed by the etched microrods, the regular microrods and the double overgrowth sample, which has the highest NBE energy. The stripe sample exhibits the largest energy shift compared with the three other samples, which have peak energies much closer together as indicated by the arrows in figure 4(a). A shift to lower energies (redshift) could have two strain-related causes, either a reduction in compressive strain or an increase in tensile strain. It all depends on the strain state with respect to the unstrained case. The strain in the etched microrod and stripe samples have been investigated in [22, 23] by recording reciprocal space maps using HRXRD. It was found that the etched microrods are less compressively strained in both in-plane directions compared with the as-grown GaN layer. The stripe sample on the other hand exhibited even less compressive strain in the *c*-direction, but larger tensile strain in the *a*-direction compared with either the etched microrod or as-grown samples. This would be consistent with the decrease in NBE emission energy observed in figure 4(a) for the stripe sample compared with the etched microrod sample. Jiu *et al* [22] also reported on the full width at half maximum (FWHM) of the HRXRD rocking curve which is a measure of the crystal quality. The FWHM increases in the following order: stripes $>$ etched microrods $>$ double overgrowth. The NBE energy on the other hand shows the exact opposite trend for these microstructures. This relationship between emission energy and HRXRD FWHM

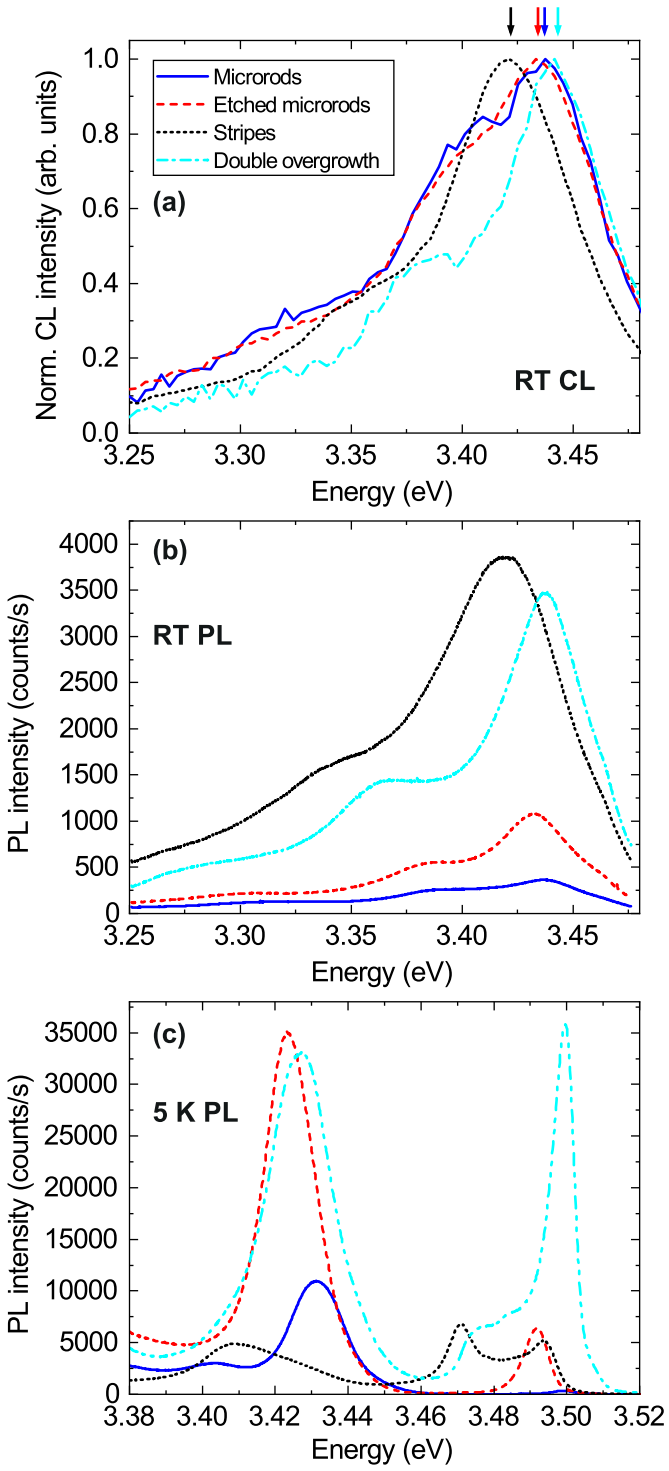

Figure 4. Luminescence spectra of the four different overgrown microstructures: (a) RT CL spectra normalised to the GaN NBE emission. The CL spectra were generated from the hyperspectral data set also used for generating the GaN NBE intensity images in figures 2(e)–(h). The approximate position of the NBE peak is marked by arrows. PL spectra at (b) RT and (c) low temperature (5 K).

is consistent with the general observation for GaN, namely a decrease in emission energy with increasing FWHM [27].

The lower energy shoulder peaks are most dominant for the two microrod samples and decrease in strength for the stripe and double overgrowth samples. These lower energy shoulders are the remnants of the SF emission at RT since the SF-related emission has mostly thermalised at these temperatures [18, 28, 29], implying that these two samples have a higher SF density. SFs cause non-radiative recombination at RT and their effect can be seen in the CL intensity images in figures 2(e) and (f) for the two microrod samples which exhibit larger darker areas. On the other hand the stripe and double overgrowth samples in figures 2(g) and (h) show more brighter areas and reduced shoulder emission implying a lower SF density.

RT PL measurements for the four samples are shown in figure 4(b). The samples were placed next to each other in order to assess their relative emission intensities and hence relate this to their crystal quality. As expected, the samples overgrown on the regular microrods have the lowest intensity. The PL intensity increases for the etched microrod sample, where defect propagation was suppressed by etching the $-c$-side of the microrod. The highest intensity is observed for the stripe sample. In contrast to the XRD measurement in [23], the double overgrowth sample with the smallest FWHM only exhibits the second highest intensity. However, it is very close to the stripe sample and both intensities are much higher compared with both microrod samples.

In order to further assess the presence of SFs, PL measurements at low temperature (5 K) were performed. At low temperature SFs cause distinctive emission peaks around 3.4 eV, which can be observed for all four samples as seen in figure 4(c) in addition to the bound exciton peak around 3.49 eV. The SF emission at low temperature is similarly affected by electric fields and strain as the emission from quantum wells, which causes the peak to shift slightly [29]. Additionally, n-type doping around the SF is also known to shift its emission energy [30], although it should be noted that the samples are nominally undoped.

The intensity ratio of the bound exciton emission and SF peak is often used to provide a relative measure of SF density. For the two microrod-patterned samples, the SF emission is much more intense compared with the bound exciton emission: about 38 $\times$ and 5 $\times$ for the regular microrod and etched microrod sample, respectively. This shows again that the etching on the $-c$-side of the microrod suppresses the propagation of defects during the overgrowth. On the other hand, for the two samples using stripes the intensity of the SF emission is comparable with the bound exciton line. The double overgrowth samples shows bound exciton emission 1.2 $\times$ higher than the SF peak, whereas for the stripe sample it is slightly weaker by a factor of 0.9 $\times$. It is also noteworthy that the stripe sample shows an additional peak around 3.47 eV, a similar shoulder peak is present for the double overgrowth sample as well. The origin of this line is not clear, but possibly related to a bound exciton bound to another defect or impurity.

4. Conclusions

In summary, the influence of different types of template micro-patterns on the luminescence and defect properties of non-polar $(11\bar{2}0)$ GaN was investigated. These micro-patterns

were a regular microrod array, etched microrods, etched stripes and a combination of stripes and microrods (double overgrowth). The samples using microrods exhibit large dark regions of reduced GaN NBE intensity associated with non-radiative recombination at TDs and SFs as identified by RT CL imaging. Using stripes improved the emission uniformity and only periodic and narrow dark bands related to the stripe patterning are present. Similarly, the lower energy shoulders on the RT NBE emission, which are related to SFs, are strongly reduced for the samples employing stripes. Low temperature PL showed a reduction in intensity of the SF-related emission line with respect to the bound exciton emission when using stripes or the double overgrowth. This indicates a reduction in SF density when employing the stripes for the overgrowth compared with microrods. Anisotropic strain relaxation in these non-polar GaN layers also impacts the emission energy as observed in the luminescence measurements. CL imaging showed that the choice of patterned microstructure used for the overgrowth of non-polar GaN has a strong impact on the presence of defects and the spatial uniformity of the luminescence. Using the right microstructure can reduce the defect density and lead to more uniform emission of light emitting semiconductors.

Acknowledgments

The authors would like to thank UK EPSRC (Grant Nos. EP/M003132/1, EP/M015181/1, EP/P015719/1 and EP/P006973/1) for financial support. J Bruckbauer acknowledges the support of SUPA through a PECRE travel award. The data associated with this research are available at https://doi.org/10.15129/feded221-778b-4eae-8cf3-5322a3aec763 or from the corresponding author.

ORCID iDs

Jochen Bruckbauer https://orcid.org/0000-0001-9236-9320
Ling Jiu https://orcid.org/0000-0001-5014-297X
Jie Bai https://orcid.org/0000-0002-6953-4698
Carol Trager-Cowan https://orcid.org/0000-0001-8684-7410
Robert W Martin https://orcid.org/0000-0002-6119-764X

References

[1] Tsao J Y, Crawford M H, Coltrin M E, Fischer A J, Koleske D D, Subramania G S, Wang G T, Wierer J J and Karlicek R F 2014 *Adv. Opt. Mater.* **2** 809
[2] Bernardini F, Fiorentini V and Vanderbilt D 1997 *Phys. Rev.* B **56** R10024
[3] Takeuchi T, Sota S, Katsuragawa M, Komori M, Takeuchi H, Amano H and Akasaki I 1997 *Jpn. J. Appl. Phys.* **36** L382
[4] Fujiwara T, Yeluri R, Denninghoff D, Lu J, Keller S, Speck J S, DenBaars S P and Mishra U K 2011 *Appl. Phys. Express* **4** 096501
[5] Marchand H, Wu X H, Ibbetson J P, Fini P T, Kozodoy P, Keller S, Speck J S, DenBaars S P and Mishra U K 1998 *Appl. Phys. Lett.* **73** 747
[6] Vennéguès P, Beaumont B, Bousquet V, Vaille M and Gibart P 2000 *J. Appl. Phys.* **87** 4175
[7] Haskell B A *et al* 2003 *Appl. Phys. Lett.* **83** 644
[8] Bougrioua Z, Laügt M, Vennéguès P, Cestier I, Gühne T, Frayssinet E, Gibart P and Leroux M 2007 *Phys. Status Solidi* A **204** 282
[9] Zhang Y, Bai J, Hou Y, Yu X, Gong Y, Smith R M and Wang T 2016 *Appl. Phys. Lett.* **109** 241906
[10] Wang T 2016 *Semicond. Sci. Technol.* **31** 093003
[11] Albert S, Bengoechea-Encabo A, Zuniga-Perez J, de Mierry P, Val P, Sanchez-Garcia M A and Calleja E 2014 *Appl. Phys. Lett.* **105** 091902
[12] Albert S, Bengoechea-Encabo A, Lopez-Romero D, de Mierry P, Zúñiga-Pérez J, Kong X, Trampert A, Sanchez-Garcia M and Calleja E 2015 *Proc. SPIE* **9370** 254
[13] Rosner S J, Carr E C, Ludowise M J, Girolami G and Erikson H I 1997 *Appl. Phys. Lett.* **70** 420
[14] Bruckbauer J, Edwards P R, Wang T and Martin R W 2011 *Appl. Phys. Lett.* **98** 141908
[15] Naresh-Kumar G *et al* 2014 *Microsc. Microanal.* **20** 55
[16] Albrecht M, Weyher J L, Lucznik B, Grzegory I and Porowski S 2008 *Appl. Phys. Lett.* **92** 231909
[17] Massabuau F C P, Bruckbauer J, Trager-Cowan C and Oliver R A 2019 Microscopy of defects in semiconductors *Characterisation and Control of Defects in Semiconductors* (London: Institution of Engineering and Technology) p 345
[18] Trager-Cowan C *et al* 2019 *Photon. Res.* **7** B73
[19] Ranalli F, Parbrook P J, Bai J, Lee K B, Wang T and Cullis A G 2009 *Phys. Status Solidi* c **6** S780
[20] Gühne T, Bougrioua Z, Vennéguès P, Leroux M and Albrecht M 2007 *J. Appl. Phys.* **101** 113101
[21] Bai J, Gong Y, Xing K, Yu X and Wang T 2013 *Appl. Phys. Lett.* **102** 101906
[22] Jiu L, Gong Y and Wang T 2018 *Sci. Rep.* **8** 9898
[23] Bai J, Jiu L, Gong Y and Wang T 2018 *Semicond. Sci. Technol.* **33** 125023
[24] Paskova T, Darakchieva V, Paskov P, Birch J, Valcheva E, Persson P, Arnaudov B, Tungasmitta S and Monemar B 2005 *J. Cryst. Growth* **281** 55
[25] Edwards P R, Jagadamma L K, Bruckbauer J, Liu C, Shields P, Allsopp D, Wang T and Martin R W 2012 *Microsc. Microanal.* **18** 1212
[26] Chen C Q *et al* 2005 *Phys. Status Solidi* c **2** 2732
[27] Kisielowski C *et al* 1996 *Phys. Rev.* B **54** 17745
[28] Corfdir P *et al* 2009 *J. Appl. Phys.* **105** 043102
[29] Lähnemann J, Jahn U, Brandt O, Flissikowski T, Dogan P and Grahn H T 2014 *J. Phys. D: Appl. Phys.* **47** 423001
[30] Hocker M, Tischer I, Neuschl B, Thonke K, Caliebe M, Klein M and Scholz F 2016 *J. Appl. Phys.* **119** 185703